Original Research

Increase in the Iron Content of the Substantia Nigra and Red Nucleus in Multiple Sclerosis and Clinically Isolated Syndrome: A 7 Tesla MRI Study

Anna I. Blazejewska, PhD,[1] Ali M. Al-Radaideh, PhD,[2] Sam Wharton, PhD,[1] Su Yin Lim, PhD,[3] Richard W. Bowtell, PhD,[1] Cris S. Constantinescu, PhD,[3] and Penny A. Gowland, PhD[1]*

Purpose: To study iron deposition in the substantia nigra (SN) and red nuclei (RN), in patients with clinically isolated syndrome (CIS) and relapsing remitting MS (RRMS) and healthy controls (HC).

Materials and Methods: Iron deposition was assessed using susceptibility maps and T2*-w images acquired at high resolution MRI at 7 Tesla (T). Mean intensities were calculated within circular regions of interest in the SN (d/v, dorsal/ventral) and RN on high resolution T2*-w, quantitative susceptibility maps and their product for: RRMS, CIS and HC (N = 14, 21, 27, respectively).

Results: Magnetic susceptibility was significantly greater in SNd and RN in RRMS compared with HC ($P = 0.04$ [0.001, 0.48] and $P = 0.01$ [0.005, 0.05]), with intermediate values for the CIS group. 1/T2*-w did not show significant inter-group differences (for SNv, SNd, RN, respectively: $P = 0.5$ [−0.352, 0976], $P = 0.35$ [−0.208, 0.778], $P = 0.16$ [−0.114, 0.885] for RRMS versus HC) and the T2*-susceptibility product maps showed the difference only for RN ($P = 0.01$, [0.009, 0.062]). Changes were independent of EDSS and disease duration.

Conclusion: MR changes consistent with iron accumulation occurring in the SN and RN of CIS patients can be identified using susceptibility mapping; this may provide an additional method of monitoring early MS development.

Key Words: multiple sclerosis; clinically isolated syndrome; magnetic resonance imaging; gray matter; substantia nigra; red nucleus
J. Magn. Reson. Imaging 2015;41:1065–1070.

CONVENTIONAL MRI TECHNIQUES which are sensitive to white matter (WM) lesions, such as fluid-attenuated inversion recovery (FLAIR), T2-weighted and post contrast T1-weighted sequences, are established methods for diagnosing and monitoring multiple sclerosis (MS) (1). However, these lesions show poor correlation with the clinical status of the disease and weak predictive value for its long-term prognosis (2,3). New quantitative MRI techniques along with the increased spatial resolution provided by high field MRI allow detection of pathology in normal appearing WM as well as in cortical and deep gray matter (GM), redefining MS as no longer an exclusively WM disease (4). Better knowledge of the gray matter involvement could improve our understanding of the pathogenesis of MS and may provide new biomarkers for disease prognosis.

Iron accumulation is often associated with neurodegeneration and can be monitored in vivo with MRI using T2- and T2*-weighted scans, or R2 or R2* maps (5–11) which provide more quantitative measures (12). However these NMR relaxation based parameters are also sensitive to the compartmentalization of iron and other tissue properties such as myelin content and water concentration (13), which can change in neurodegeneration. Recent studies have used phase data to obtain information more specifically related to iron content (14) and susceptibility weighted images (SWI) combining phase and T2*-weighted signals with the aim of achieving higher sensitivity to iron density (15,16). However the phase maps and hence SWI data are distorted compared with the underlying susceptibility distribution in the tissue because there is a nonlocal relationship between the susceptibility distribution and the resulting magnetic field distortion. We have taken an alternative approach using quantitative susceptibility mapping (17–20) which converts phase data into magnetic susceptibility maps that are not spatially distorted.

In MS MRI changes suggestive of increased iron content have been reported for most of the deep gray matter (dGM) structures, including putamen, thalamus, substantia nigra, red nucleus, head of caudate

[1]Sir Peter Mansfield Magnetic Resonance Centre, School of Physics and Astronomy, University of Nottingham, United Kingdom.
[2]Department of Medical Imaging, Faculty of Allied Health Sciences, Hashemite University, Zarqa, Jordan.
[3]Division of Clinical Neurology, School of Clinical Sciences, University of Nottingham, United Kingdom.
Contract grant sponsor: Xxxxxxx; Contract grant number: xxxxxxxx.
*Address reprint requests to: P.A.G., SPMMRC, School of Physics and Astronomy, University of Nottingham, University Park, NG7 2RD, Nottingham, UK. E-mail: penny.gowland@nottingham.ac.uk
Received December 4, 2013; Accepted April 4, 2014.
DOI 10.1002/jmri.24644
View this article online at wileyonlinelibrary.com.

nucleus, globus pallidus, and dentate nucleus (10,16,21,22). However results of iron depsosition in the substantia nigra (SN) and red nucleus (RN) remain inconsistent: while some studies reported a difference between MS and healthy subjects in both structures (8,11,12), others found increased iron only in the SN (23,24) or only in the RN (6) and some studies reported no difference in either (5,9). The brainstem is commonly involved in MS and is associated with poor prognosis possibly due to its engagement in motor control (20,25). Lesions of the RN including demyelinating plaques within it or affecting its connection to the cerebellum may cause a characteristic rubral tremor (26). In addition, involvement of the SN in MS has been demonstrated through the detection of lesions on transcranial sonography (27) and decreased levels of proteins associated with myelin, neuronal development, and axonal growth indicating demyelination of the SN (24).

In clinically isolated syndrome (CIS, a condition indicating the earliest clinical stage of demyelinating disease), previous MRI studies of iron accumulation in dGM structures often excluded the SN and RN (8,10). We have recently reported significant differences in susceptibility mapping based measures of iron content of dGM structures (caudate nucleus, putamen, globus pallidus, thalamus, and pulvinar) between CIS patients and healthy controls, but failed to include the brain stem regions in that study (21).

Here, we extend a previous study to investigate changes in iron deposition in the SN and RN in two groups of patients, with relapsing-remitting MS (RRMS) and CIS, hypothesizing that iron deposition in the SN and RN might ultimately provide a marker of the progression of CIS to MS. The aim of this work was to assess iron content in the SN and RN of patients with CIS and RRMS compared with healthy controls (HC), using susceptibility mapping (8) which is sensitive to absolute iron content and T2*-weighted signals which depend on the compartmentalization of iron. We acquired the data using a 7 Tesla (T) MR scanner, as the field shifts due to magnetic susceptibility perturbations scale with the field strength, increasing sensitivity in both measures. Ventral (SNv) and dorsal (SNd) parts of the SN were analyzed separately based on the reported changes in iron distribution in other neurodegenerative diseases (28).

MATERIALS AND METHODS

Fourteen patients with relapsing-remitting multiple sclerosis (RRMS: age = 42.4 ± 11.3; range, 20–56 years old) and 21 with clinically isolated syndrome (CIS: age = 37.2 ± 8.8; range, 24–57 years old) together with 27 age-matched healthy controls (HC: age = 36.4 ± 8.8; range, 21–58 years old) were recruited from Nottingham University Hospital in accordance with local ethics committee approval. Expanded Disability Status Scale (EDSS) assessment giving values between 0 and 10 (death due to MS) was performed by a trained physician for all of the patients.

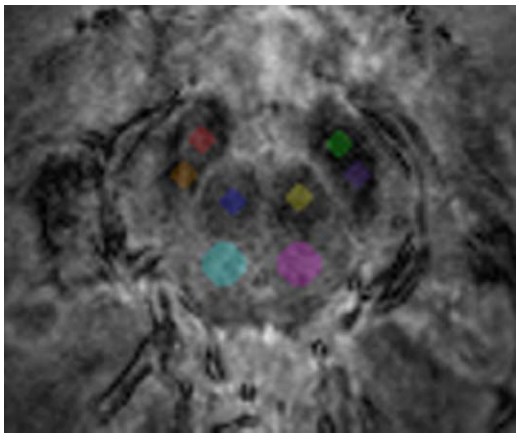

Figure 1. T2*-weighted image showing ROIs placed in the SNv (red and green), SNd (orange and purple) and RN (blue and yellow). The two ROIs in cyan and magenta are WM regions used for normalization.

MR images were acquired on a 7 T Philips Achieva scanner with 16-channel receive coil and head-only volume transmit coil. A T2*-weighted three-dimensional (3D) GRE sequence was acquired with repetition time/echo time (TR/TE) = 150/20 ms, flip angle 14°, SENSE factor 2, echo planar imaging (EPI) factor 3, number of acquisitions 1, scan time 8.5 min. Four interleaved stacks parallel to the AC-PC line with coverage 192 × 164 × 25 mm were acquired for each scan, where the overlap between stacks was 5 mm. Spatial resolution of the data was 0.5 × 0.5 × 0.5 mm.

To overcome the problem of nonlocal effects in phase maps, susceptibility maps were generated from the phase data using the thresholded *k*-space division method (17). For each subject, the five slices of each T2*-w image in which both structures were most visible were chosen and then circular regions of interest (ROIs) of diameter 3 mm were drawn by a physicist trained in the dGM anatomy using ITKSnap software (http://www.itksnap.org), separately on the left and right RN, ventral and dorsal SN (Fig. 1). All of the SN ROIs were positioned to avoid touching ventral and medial boundaries of the structure. Two further ROIs of 5 mm diameter were placed on the white matter (WM) in the same slices and used to provide reference values for the susceptibility measurements.

Matlab (The MathWorks Inc., 2010) was used for further processing of the data. Mean intensities were measured on T2*-w modulus images and susceptibility maps for SNv, SNd, and RN ROIs, and the values obtained from the left and right sides were averaged together. The results were normalized using the mean intensity of the WM region, taking the difference between the ROI and WM region for susceptibility and ratio of the ROI to the WM region for T2*-w. Moreover the product of the negative logarithm of the normalized T2*-w signal (which should be linear in 1/T2* and hence iron concentration) and normalized susceptibility signal (Susceptibility-T2* product) was determined for each structure, to increase sensitivity in a similar manner to the SWI (by combining magnitude and phase information which are independent physical measures but have reinforcing effects in the

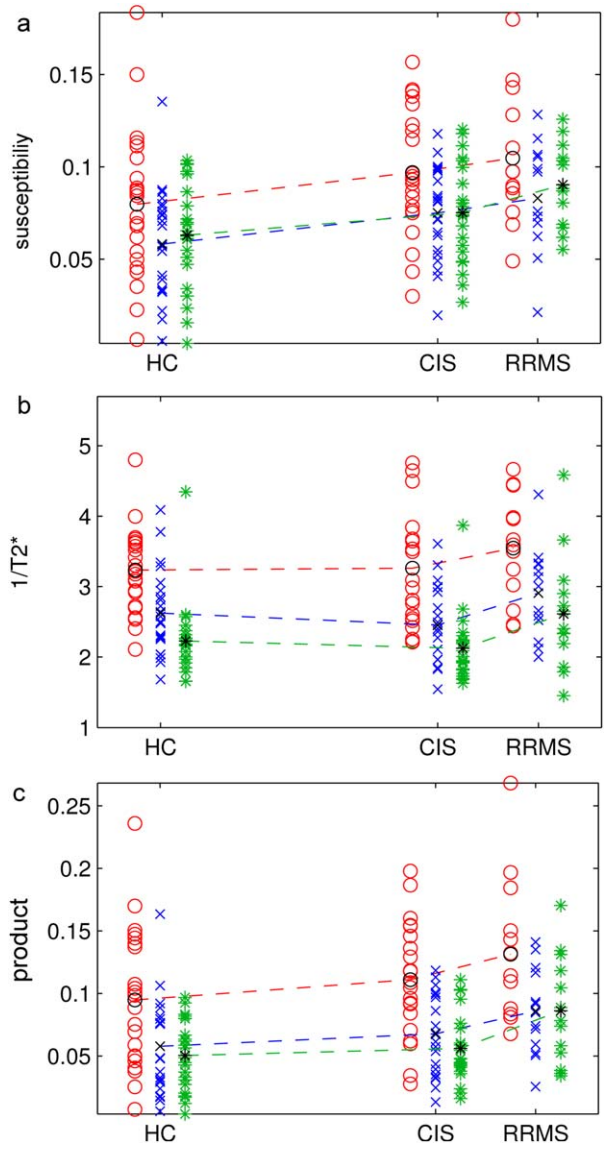

Figure 2. Mean susceptibility (a), 1/T2*-w (b), and product (c) in SNv (○), SNd (×), and RN (⋆) for HC, CIS, and RRMS patients; mean values calculated within each group plotted in black and connected by lines.

presence of iron) signal but using susceptibility maps to overcome the problems of nonlocal phase effects in SWI data.

Normality was checked using the Kolmogorov-Smirnov test. One-way analysis of variance (ANOVA) tests with the Tukey-Kramer correction for multiple comparisons were performed to examine differences in susceptibility and 1/T2*-w values between the CIS, RRMS patients, and HC for each structure. Left and right parts of the structures were also compared using one-way ANOVA. Scatter plots of susceptibility and 1/T2*-w signal were overlaid with ellipses indicating the HC, CIS and RRMS population distributions (±1.5 SD). Dependence of the 1/T2*-w, susceptibility and product values on age was tested for healthy controls and dependence on the EDSS score and disease duration for the CIS and RRMS patients.

RESULTS

Mean EDSS results obtained for the two groups of patients were 2.8 ± 0.7 for RRMS and 1.6 ± 1.0 for CIS.

There was a trend for susceptibility in all of the structures to increase between HC, CIS, and RRMS patients (Fig. 2a) and the differences between HC and RRMS in SNd and RN were significant ($P=0.04$, confidence intervals [0.001, 0.048] and $P=0.01$ [0.005, 0.05] for SNd and RN, respectively). No difference was seen in SNv although this may be because the data for this region were more scattered. The 1/T2*-w signal in both parts of the SN and RN was unchanged for CIS patients compared with HC and higher for RRMS patients, although differences were not significant (for SNv, SNd, RN: $P=0.99$, $P=0.6$, $P=0.84$, confidence intervals [−0.55, 0.60], [−0.60,0,26], [−0.54, 0.33] for HC versus CIS and $P=0.5$, $P=0.35$, $P=0.16$, [−0.35, 0.98], [−0.21, 0.78], [−0.11, 0.89] for HC versus RRMS, Fig. 2b). The Susceptibility-T2* product increased the separation of RRMS versus HC ($P=0.01$, [0.009, 0.062]) and RRMS versus CIS groups ($P=0.03$, [0.003, 0.057]) in RN; however, the difference between the groups for SNd was no longer significant ($P=0.06$, [−0.001, 0.057] for RRMS versus HC and $P=0.31$ [−0.012, 0.048] for RRMS versus CIS).

Scatter plots in Figure 3 show that there is relatively weak correlation between susceptibility and 1/T2*-w signal in all ROIs for all subject groups (correlation coefficients: 0.16, 0.34, 0.44 for SNv, SNd, and RN, respectively).

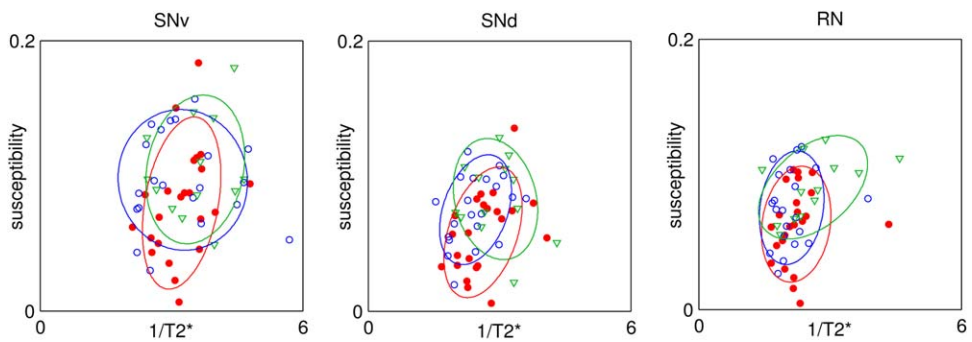

Figure 3. Scatter plots of susceptibility versus 1/T2*-w in (a) SNd, (b) SNv and (c) RN. Ellipses indicate populations of the HC (●), CIS (○), and RRMS (△) centered at the mean value, outlined by the 1.5 standard deviations and oriented parallel to the best fit slope.

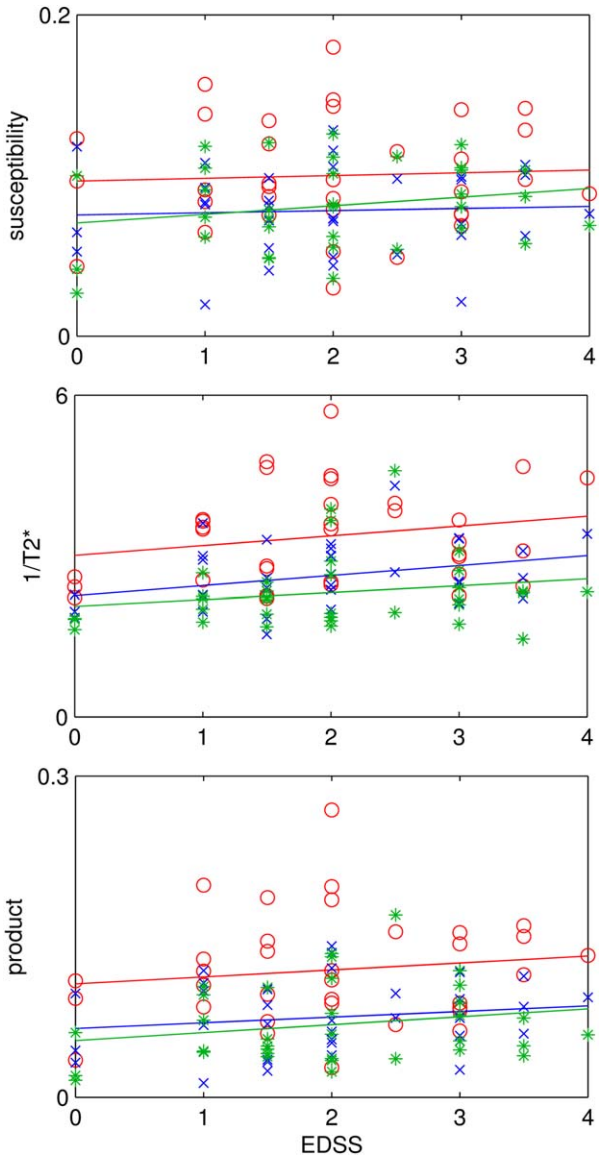

Figure 4. Values of susceptibility (a), 1/T2*-w (b), and product (c) in SNv (○), SNd (×), and RN (⋆) plotted against their EDSS scores together with lines of the best fit.

Susceptibility, 1/T2*-w, and the product did not show a significant correlation either with the patients' EDSS score (correlation coefficients and *P*-values for SNv, SNd, RN: 0.05, 0.05, 0.21, and 0.77, 0.77, 0.23 for susceptibility, 0.21, 0.31, 0.20, and 0.23, 0.07, 0.26 for 1/T2*-w and 0.1, 0.16, 0.23, and 0.46, 0.36, 0.23 for product) or disease duration as well as with age for HC (correlation coefficients and *P*-values for SNv, SNd, RN: −0.01, −0.15, 0.11 and 0.98, 0.48, 0.62 for susceptibility, 0.30, 0.15, 0.39, and 0.17, 0.51, 0.07 for 1/T2* and 0.09, −0.05, 0.25, and 0.69, 0.82, 0.25 for product) and no significant differences between the left- and right side- structures were found (Fig. 4).

DISCUSSION

Changes consistent with increased iron content in the SNd and RN were found in RRMS patients compared with HCs using susceptibility mapping at 7T. There was a trend for the CIS patients to have higher values than HC in all three ROIs, although the differences were not significant. These results suggest a relationship between iron deposition and progression from CIS to RRMS, although because this was a cross-sectional study, it is not possible to be certain if this relates directly to conversion to RRMS. These results concord with previous work applying the same quantitative susceptibility mapping method to the other dGM structures for the same CIS patients (21). The combined measure, Susceptibility-T2* product, was affected by the difference in trends occurring in 1/T2*-w signal and susceptibility between HC and patients groups. The values of this product increased the separation of the RRMS and HC groups in comparison to susceptibility, but did not show significant differences for the CIS versus HC (as may be expected from the results on 1/T2*-w alone). However, there remained considerable overlap between the three groups for all measures, with similar spread observed for the healthy controls as for both patient groups. Nonetheless, the combined measure of iron concentration could have an advantage over susceptibility alone in monitoring CIS and MS patients.

The effects of iron accumulation on susceptibility maps and T2*-w images are different. Susceptibility will depend on the total iron content within a voxel (13). On the other hand T2*-w signal decay will depend on both the total iron content of the tissue and also its distribution (i.e., whether or not the iron is aggregated into "clumps"). Therefore, a trend for susceptibility to change earlier in demyelinating diseases (CIS) than T2*-w might suggest that iron accumulation is uniform initially but becomes more heterogeneous later. However, susceptibility and T2*-w signal also depend on myelin content (13); thus, demyelination may also explain the observed differences in the changes in T2*-w and susceptibility between groups. Myelin is diamagnetic (negative susceptibility), whereas iron is paramagnetic (positive susceptibility). Hence, both demyelination and increased iron content would be manifested as a net increase in susceptibility. In contrast, myelin generally reduces T2 so demyelination will cause a decrease in 1/T2*-w where increased iron will cause an increase in 1/T2*-w. Further work is required to separate these effects but either way the early changes may make susceptibility mapping potentially useful in the future for monitoring progression of CIS.

We have recently reported that the nigrosome 1, the biggest of five subgroups of dopaminergic neurons located in medial part of the SN previously identified in histology (29), is visible on 7T MRI (30) of healthy controls but not of Parkinson's disease (PD) patients (30,31). Post hoc examination of the data acquired here found no change in frequency of nigrosome detection between RMMS and CIS patients and controls.

Interestingly, in our study greater differences in susceptibility were found in SNd compared with SNv. Variation across the SN may partially explain the lack of consistency in previous studies using images acquired at lower field strengths, as high resolution imaging at

7T allowed specific ROIs to be defined within the SN. It could also suggest a similar pattern of the iron accumulation in SN to that previously found in Parkinson's disease in histology (28) and T2*-w images (32) which is in agreement with the gradient of neurodegeneration found in SN in PD patients using MRI (33). Larger scatter of the SNv values compared with SNd can be possibly explained by the individual differences in the vasculature within that region.

In PD, it has previously been shown in histology (29) and in vivo MRI (30,31) that iron is preferentially deposited in nigrosome 1 and that nigrosome 1 cannot be detected in vivo in patients. On the other hand, the presence of nigrosome 1 at the same rate in both healthy subjects and MS patients does not support that hypothesis, as a previous study showed the absence of this structure in Parkinson's patients (30).

The lack of variation in iron content observed over the age range used in our study (20–58 years) agrees with previous results that suggested significant changes only in the first 2 decades (34). As in previous studies of dGM iron in MS patients, we also found no correlation between iron and EDSS, possibly due to a relatively low range of EDSS scores (8,9).

The quantitative susceptibility mapping used in this work is a robust method providing a more direct measure of the spatial iron distribution by the actual susceptibility values overcoming the problem of nonlocal relationship between the field distortion (and hence phase of the magnetization) and susceptibility (17). Although the susceptibility maps are rather sensitive to noise, the increase of the signal-to-noise ratio in the images obtained from 7T magnetic field is sufficient to acquire good quality data. The need for a reference region will increase scatter in the data, and could potentially bias the results if there were a systematic change in the WM. However, as cerebrospinal fluid is affected by flow, WM is the most robust choice of normalization region.

Limitations of this study include the low number of subjects, especially considering certain level of intragroup heterogeneity within the patients groups. Further work should also include longitudinal analysis taking into account conversion from CIS to RRMS on the later stages of the disease. Quantitative measurement of R2* values (to replace 1/T2*-w used in this work) would give a more accurate insight in changes of iron concentration in the analyzed structures, and additional measures such as R2, the field-dependent rate increase technique, or magnetization transfer could provide further information about the changes occurring.

In this study we used quantitative susceptibility mapping to analyze iron accumulation in SN and RN in CIS and RRMS patients. Future work will include R2* and magnetization transfer measurements in longitudinal studies, will investigate whether these measures can predict conversion from CIS to RRMS.

ACKNOWLEDGMENTS

Grant support: Morris, Bowtell, Francis, Glover, Gowland, Kockenberger, Auer, Jackson, Krumbholz, Liddle, Palmer, Paus, 2009–2014. Realizing the benefits of structural and functional MRI at ultra-high-field: MRC and EPSRC (35%) £2,424,424.

REFERENCES

1. Polman CH, Reingold SC, Banwell B, et al. Diagnostic criteria for multiple sclerosis: 2010 revisions to the McDonald criteria. Ann Neurol 2011;69:292–302.
2. Barkhof F. MRI in multiple sclerosis: correlation with expanded disability status scale (EDSS). Mult Scler 1999;5:283–286.
3. Kappos L, Moeri D, Radue EW, et al. Predictive value of gadolinium-enhanced magnetic resonance imaging for relapse rate and changes in disability or impairment in multiple sclerosis: a meta-analysis. Gadolinium MRI Meta-analysis Group. Lancet 1999;353:964–969.
4. Filippi M, Rocca MA, De Stefano N, et al. Magnetic Resonance Techniques in Multiple Sclerosis. Arch Neurol 2011;68:1514–1520.
5. Drayer B, Burger P, Hurwitz B, et al. Reduced signal intensity on MR images of thalamus and putamen in multiple sclerosis: increased iron content? AJR Am J Roentgenol 1987;149:357–363.
6. Bakshi R, Benedict RHB, Bermel RA, et al. T2 Hypointensity in the deep gray matter of patients with multiple sclerosis. Arch Neurol 2002;59:62–68.
7. Khalil M, Enzinger C, Langkammer C, et al. Quantitative assessment of brain iron by R(2)* relaxometry in patients with clinically isolated syndrome and relapsing-remitting multiple sclerosis. Mult Scler 2009;15:1048–1054.
8. Zhang Y, Zabad RK, Wei X, et al. Deep grey matter "black T2" on 3 Tesla magnetic resonance imaging correlates with disability in multiple sclerosis. Mult Scler 2007;13:880–883.
9. Zhang Y, Metz LM, Yong VW, et al. 3T deep gray matter T2 hypointensity correlates with disability over time in stable relapsing-remitting multiple sclerosis: a 3-year pilot study. J Neurol Sci 2010;297:76–81.
10. Ceccarelli A, Rocca MA, Neema M, et al. Deep gray matter T2 hypointensity is present in patients with clinically isolated syndromes suggestive of multiple sclerosis. Mult Scler 2010;16:39–44.
11. Pawate S, Wang L, Song Y, et al. Analysis of T2 intensity by magnetic resonance imaging of deep gray matter nuclei in multiple sclerosis patients: effect of immunomodulatory therapies. J Neuroimaging 2011;22:137–144.
12. Lebel RM, Eissa A, Seres P, et al. Quantitative high-field imaging of sub-cortical gray matter in multiple sclerosis. Mult Scler 2012;18:433–441.
13. Haacke EM, Cheng NYC, House MJ, et al. Imaging iron stores in the brain using magnetic resonance imaging. Magn Reson Imaging 2005;23:1–25.
14. Hammond KE, Metcalf M, Carvajal L, et al. Quantitative in vivo magnetic resonance imaging of multiple sclerosis at 7 Tesla with sensitivity to iron. Ann Neurol 2008;64:707–713.
15. Haacke EM, Mittal S, Wu Z, et al. Susceptibility-weighted imaging: technical aspects and clinical applications, part 1. AJNR Am J Neuroradiol 2009;30:19–30.
16. Zivadinov R, Heininen-Brown M, Schirda CV, et al. Abnormal subcortical deep-gray matter susceptibility-weighted imaging filtered phase measurements in patients with multiple sclerosis: a case-control study. Neuroimage 2012;59:331–339.
17. Wharton S, Schafer A, Bowtell R. Susceptibility mapping in the human brain using threshold-based k-space division. Magn Reson Med 2010;63:1292–1304.
18. Liu T, Spincemaille P, De Rochefort L, et al. Calculation of susceptibility through multiple orientation sampling (COSMOS): a method for conditioning the inverse problem from measured magnetic field map to susceptibility source image in MRI. Magn Reson Med 2009;61:196–204.
19. Schweser F, Deistung A, Lehr BW, et al. SEMI-TWInS: Simultaneous extraction of myelin and iron using a T2*-weighted imaging sequence. Proc. ISMRM 19 2011;104.
20. Damasceno A, Von Glehn F, Brandao CO, et al. Prognostic indicators for long-term disability in multiple sclerosis patients. J Neurol Sci 2013;324:29–33.
21. Al-Radaideh AM, Wharton SJ, Lim S-Y, et al. Increased iron accumulation occurs in the earliest stages of demyelinating disease:

an ultra-high field susceptibility mapping study in clinically isolated syndrome. Mult Scler 2012;19:896–903.
22. Quinna MP, Gatib JS, Klassenb ML, et al. Increased deep gray matter iron is present in clinically isolated syndromes. Mult Scler Relat Disord (in press).
23. Haacke EM, Garbern J, Miao Y, et al. Iron stores and cerebral veins in MS studied by susceptibility. Int Angiol 2010;29:149–157.
24. Chen X, Zeng C, Luo T, et al. Iron deposition of the deep grey matter in patients with multiple sclerosis and neuromyelitis optica: a control quantitative study by 3D-enhanced susceptibility-weighted angiography (ESWAN). Eur J Radiol 2012;81:e633–e639.
25. Tintore M, Rovira A, Arrambide G, et al. Brainstem lesions in clinically isolated syndromes. Neurology 2010;75:1933–1938.
26. Koch M, Mostert J, Heersema D, et al. Tremor in multiple sclerosis. J Neurol 2007;254:133–145.
27. Horowski S, Zettl UK, Benecke R, et al. Sonographic basal ganglia alterations are related to non-motor symptoms in multiple sclerosis. J Neurol 2011;258:195–202.
28. Fearnley JM, Lees AJ. Ageing and Parkinson's disease: substantia nigra regional selectivity. Brain 1991;114:2283–2301.
29. Damier P, Hirsch EC, Agid Y, et al. The substantia nigra of the human brain II. Patterns of loss of dopamine-containing neurons in Parkinson's disease. Brain 1999;122:1437–1448.
30. Blazejewska AI, Schwarz ST, Pitiot A, et al. Visualization of nigrosome 1 and its loss in PD: Pathoanatomical correlation and in vivo 7 T MRI. Neurology 2013;81:534–540.
31. Kwon D-H, Kim J-M, Oh S-H, et al. Seven-Tesla magnetic resonance images of the substantia nigra in Parkinson disease. Ann Neurol 2012;71:267–277.
32. Lotfipour AK, Wharton S, Schwarz ST, et al. High resolution magnetic susceptibility mapping of the substantia nigra in Parkinson's disease. J Magn Reson Imaging 2012;35:48–55.
33. Minati L, Grisoli M, Carella F, et al. Imaging degeneration of the substantia nigra in Parkinson disease with inversion-recovery. AJNR Am J Neuroradiol 2007;28:309–313.
34. Hallgren B, Sourander P. The effect of age on the non-heamin iron in the human brain. J Neurochem 1958;3:41–51.